Main Article

Fragility curves for road embankments exposed to adjacent debris flow

Progress in Physical Geography
2022, Vol. 0(0) 1–18

DOI: 10.1177/03091333221111444
journals.sagepub.com/home/ppg
SAGE

Natalia Nieto and Alondra Chamorro
Department of Construction Engineering and Management, School of Engineering, Pontificia Universidad Católica de Chile, Santiago, Chile; Research Center for Integrated Disaster Risk Management (CIGIDEN), Santiago, Chile; Latin American Center for Economic and Social Policies (CLAPES UC), Pontificia Universidad Católica de Chile, Santiago, Chile

Tomás Echaveguren
Department of Civil Engineering, Faculty of Engineering, Universidad de Concepción, Concepción, Chile; Research Center for Integrated Disaster Risk Management (CIGIDEN), Santiago, Chile

Cristián Escauriaza
Department of Hydraulic and Environmental Engineering, Pontificia Universidad Católica de Chile, Santiago, Chile; Research Center for Integrated Disaster Risk Management (CIGIDEN), Santiago, Chile

Abstract

Studies of recent decades have shown thousands of kilometers of transportation networks that have presented damage or failure from different types of flows, causing important traffic disruptions. Debris flows running adjacent (or in parallel) to river channels often explain the structural damage to road embankments caused by slope erosion. The probability of expected structural damage caused by a natural hazard may be modeled using fragility curves, which have been developed for transportation infrastructures like bridges and roads exposed to debris flows and are used in risk assessment. There are even fragility curves available to estimate the fragility of road embankments exposed to perpendicular debris flows. However, currently no model is available to estimate the road damage probability of embankments exposed to adjacent debris flows despite their important effects on traffic. This paper aimed to develop fragility curves for road embankments exposed to adjacent debris flows, considering mechanisms of exposed slopes subject to erosion and subsequent embankment instability. Models were calibrated considering flow characteristics in straight and bend channels including three damage states in terms of road traffic capacity loss. Monte Carlo simulations were performed to model potential damage, obtaining fragility curves for two types of roads. Curves were fit to log-normal distributions with a 99.5% confidence level. The analysis demonstrated that the geometric characteristics of road embankments explain their fragility, wherein lower heights and platform widths result in more probable expected damage. The analytical model developed confirmed that the erosive process intensifies in bend zones of channels, resulting in higher damage probability.

Corresponding author:
Alondra Chamorro, Department of Construction Engineering and Management, School of Engineering, Pontificia Universidad Católica de Chile, Av. Vicuña Mackenna 4860, Santiago 7820244, Chile.
Email: achomorro@ing.puc.cl

Keywords
Fragility curves, road embankments, debris flows, riverbanks, erosion mechanisms

Introduction

Transport systems are highly vulnerable to natural hazards, and the physical damage that they generate may cause significant traffic disruption and socioeconomic impact (Argyroudis et al., 2019). Floods and debris flows lead most of these impacts, including the cost of delays and diversions on transport networks, the severance of access to relatively remote communities; employment, health, and educational opportunities (Meyer et al., 2015; Scott et al., 2006; Winter et al., 2019). In Scotland, for example, between 2004 and 2014, roads were affected by flood and debris flow events, having direct economic impacts of around US$6 million, including the emergency response and remedial works (Winter et al., 2019). The mountainous basins collect most of the natural water flow and sediments, which often affect road networks due to rapid debris flows or river flood (Meyer et al., 2015). Research developed in 2005 showed that around 1,191,000 km of transport networks (road and rail) have been exposed to floods worldwide since 1993 (Dilley et al., 2005; Meyer et al., 2015).

Debris flows are a type of landslide characterized by a mixture of sediments, rocks, different types of debris, and variable amounts of water, which form a suspension flowing downhill through ravines or river channels (Jakob and Hungr, 2005; Takahashi, 2014). These events often occur simultaneously with floods (Hungr et al., 2014) and may generate scour due to high river levels, slope erosion, instability of slope embankment, failure, and falls (Argyroudis et al., 2019). In areas of high susceptibility to the generation of debris flows events and floods, these phenomena typically destroy roads located near river channels at low elevations (Zou et al., 2018). When the road embankment is near or at the same level as the channel, it acts as the riverbank and is subject to erosive actions of flows. If embankments do not have protection systems such as gabions or riprap, the embankment slope is directly exposed to the stresses produced by high velocities and water height. Erosion in riverbanks has been studied previously regarding models of bank, stability, and toe erosion, such as in the BSTEM (Bank Stability and Toe Erosion Model) proposed by Simon et al. (2000), which considers the interaction between hydrodynamic forces and bank material. Bank erosion is produced by the shear stress exerted by the flow, which is increased in bend zones due to secondary currents generated by cross-stream pressure gradients (Crosato, 2007; Midgley et al., 2012). Road embankments are consequently damaged by flows because a complete or part of a road is lost, reducing the traffic capacity. Physical damage is related to the reduction level of service of the affected component and the corresponding functionality loss in terms of road traffic capacity (Pitilakis et al., 2014).

Given the usefulness and importance of road networks in connecting places and enabling efficient movement of people and commodities under good road conditions, it is crucial to minimize the risk and damage that embankment presents under such conditions (Tacnet et al., 2012). Risk assessment of road networks provides information that enables understanding, responding, and taking preventative actions by authorities, allocating optimal resources, and mitigating the calculated risk (Calvo and Savi, 2009; Dowling and Santi, 2014; Santi et al., 2010). One of the dimensions that consider the risk assessment and the quantification of vulnerability of infrastructures is developing probabilistic models called fragility curves to estimate infrastructure damage in terms of decreased capacity (Pitilakis et al., 2014; Peduto et al., 2017). Bridges are one of the most studied road infrastructures in the fragility curves field, for example, Kim et al. (2017), who developed fragility curves for flooded bridges. Dagá et al. (2018) considered the analysis and development of failure curves for bridge deck sliding and overturning pier due to exposure to volcanic lahar flows. Liang and Xiong (2019) developed fragility curves for bridge sliding subjected to debris flows. Other authors have considered roads and embankments exposed to different hazards, for example, for seismic hazard Argyroudis and Kaynia (2015) developed fragility curves for highways and railways on embankments and cuts due to seismic shaking using a numerical approach. Then, Oblak et al. (2020) obtained fragility curves for traffic embankments

exposed to earthquake-induced liquefaction using permanent vertical displacement as the damage parameter, and Shinoda et al. (2021) propose a seismic fragility estimation equation for embankments with the level of seismic energy calculated from the time history of ground accelerations in Japan. On the other hand, Gouldby et al. (2009) developed a methodology to evaluate the risk of flooding from river sources, considering the failure of earth embankment defense through fragility curves. In the field of roads exposed to debris flows, Winter et al. (2013, 2014) have developed fragility curves that considered the capacity loss of roads in terms of surface damage. McKenna et al. (2021) derived fragility curves for granular highway embankments subjected to flooding, considering the moisture ingress and scour generation at a vertical displacement at the road surface. Nieto et al. (2021) propose models of road embankment damage exposed to perpendicular debris flows, leaving a research gap open about models corresponding to an adjacent exposure, which means embankment erosion caused by debris flows (or clear water flows) running along a watershed where the road runs mostly parallel to the stream. This study aims to help fill that heretofore unstudied area in embankment failure.

Despite the substantial increase in research focused on quantifying transport infrastructure vulnerability, the existing models are limited and focus mainly on bridges (Argyroudis et al., 2018). Also, the debris flow phenomena over roads have been focused primarily on platforms damage. Available models do not assess the probability of physical damage caused by debris flows running adjacent to road embankments. This research aims to develop fragility curves for road embankments exposed to adjacent flows in straight and bend zones of channels in terms of reducing the operational traffic capacity of the road. A damage model is proposed for the erosion generated by flow along the embankment slope and the subsequent instability of the block that forms, considering a unit portion of the road. The model scope includes erosion generated by water flows or floods (with sediment concentration close to 0%) to debris flows (with sediment concentration less than 80%). A limit state function, the mathematical relationship that considers the demand stresses of the falling block with the resistance stresses of soil friction, is defined. The variability of the natural hazard and the embankment behavior are incorporated through Monte Carlo simulations. The above model assigns deterministic values or probabilistic distributions to the model variables. Finally, log-normal distributions are adjusted with 99.5% confidence level to the curves obtained in terms of flow height. The scope of this study includes erosion caused by debris flows in straight and bend zones of river channels near two types of roads: two-lane rural roads and multilane roads.

Effects of road embankment erosion

Erosion phenomena in road embankments affected by adjacent flows. Road networks inevitably pass

Figure 1. Examples of two-lane rural road embankments exposed to adjacent flows in Chile show considerable damage due to flow erosion. Left: Road embankment damaged by debris flow. Right: Road embankment damaged by flood. For interpretation of the references to colours in this figure legend, refer to the online version of this article.

through different types of natural geographical relief (Zou et al., 2018). In many of these cases, the roads are located adjacent to rivers or channels (see Figure 1) with the embankments originating in the riverbank and often forming part or all of that bank, and the road embankment erosion is caused by flows running along this watershed. Such channels may be constantly active and carry clear water flows under normal conditions, but they can also be dry and with necessary activation conditions, such as heavy rainstorms, can be re-activated with either water flows or debris flows if sediments and debris are available in the channel beds to be dragged and carried by the fluid (Nettleton et al., 2005; Skilodimou and Bathrellos, 2016).

Road embankments without river protection expose their infrastructure to the erosive forces the flow exerts on the embankment slope (Zou et al., 2018). With erosion, the material forming the embankment is lost, most often leaving a weak higher portion above the base, which eventually falls by its own weight. The above destruction is frequent on banks composed of fine and coarse grains activated by flows (Watson and Basher, 2006).

The interaction between the road embankment and the adjacent flows can initially cause physical damage to it, which can be measured in terms of the volume of soil or the width of the embankment crown that is lost as a result of erosion. This embankment crown width is the most practical measure because it can be easily compared with the initial width of the road. With the loss of part of the embankment due to erosion, the traffic of the affected lane is closed, and the velocity of circulation is reduced, so the road decreases its traffic capacity. Road traffic capacity corresponds to the maximum vehicle rate that can pass through a uniform section of lane or road (TRB, 2016). Physical damage is related to the level of service of the component and the corresponding functionality of the infrastructure. In the case of roads, this functionality is associated with the number of traffic lanes available (Argyroudis and Kaynia, 2014). Therefore, the physical damage to a road embankment imposes a loss in transport capacity, which has operational consequences on the road, such as traffic disruption due to the decrease in the number of lanes available and restricted circulation in terms of velocity. In turn this restriction has real economic and social consequences.

Bank erosion modeling

The erosion and loss of material from an embankment are similar to the bank erosion and lateral channel migration generated by water flows in rivers. The bank retreat mechanism considered is fluvial erosion, and then episodic mass failure mechanisms like cantilever planar, rotational, and seepage-induced failures can occur (Motta et al., 2012). One of the most common and advanced bank stability models is the Bank Stability and Toe Erosion Model (BSTEM). This model developed by Simon et al. (2000) has two analysis modules. The first considers the toe erosion of the bank produced by the flow stresses throughout the entire height. The second module provides a bank stability analysis that considers a cantilever or planar failure resulting from the loss of material by hydraulic erosion calculated in the first module (Midgley et al., 2012; Motta et al., 2012). The model calculates the safety factor of the riverbank given the flow and bank characteristics and uses three different limit balancing methods (Midgley et al., 2012; Simon, 2010; Simon, 2011).

In zones with curvature, the outer bend induces a superelevation of the flow and secondary currents, generating an increase of velocity and hydraulic loading on the bank of the channel (Allsop et al., 2007; Crosato, 2007). Considering constant average stress created by a distribution applied on the bank, two different models are included for shear stress in straight and bend channel sections (Midgley et al., 2012). In the case of road embankments, it is useful to approximate the platform width that would be lost due to flow erosion, which can be associated with operational consequences on the roads, enabling simplified analysis developed in the BSTEM. Planar failure is often considered the predominant mode of failure, resulting in the collapse of an outstanding block over the channel (Lai, 2017; Motta et al., 2012; Simon, 2010). This is also supported by empirical evidence; so, in this research, planar failure will be assumed, which is illustrated later in Figure 2.

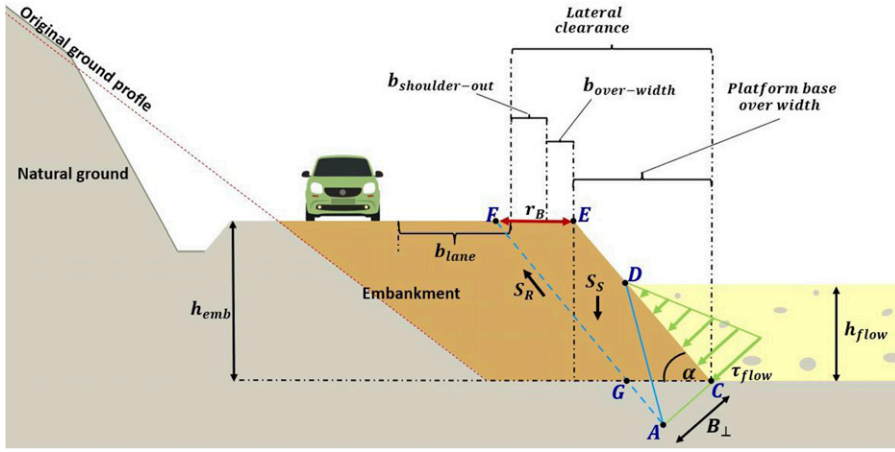

Figure 2. Damage diagram for road embankment exposed to erosion and block instability. For interpretation of the references to colours in this figure legend, refer to the online version of this article.

Intensity measure for the development of fragility curves

The fragility curves express the probability of exceeding different limit damage states as a function of some measure of excitement or natural hazard intensity (Schultz et al., 2010; Pitilakis et al., 2014; Porter, 2016). The development of the curves requires the choice of an intensity measure that characterizes the power of the natural phenomenon and relates it to the response or consequence on the analyzed infrastructure (Pitilakis et al., 2014). For example, Peduto et al. (2017) used the equivalent cumulative displacement (ECD) as intensity parameter for vulnerability and fragility curves developed for buildings exposed to slow-moving landslides. Mavrouli et al. (2014) developed fragility curves for three types of slope instability, slow-moving landslides, rapid flow-type slides, and rockfalls, using as intensity measure to the slide displacement, the flow velocity, and the diameter and kinetic energy of the rock block, respectively. For the debris flow hazard, the flow intensity has been considered as moment flux (height by squared velocity), for example, in the fragility curves developed by Prieto et al. (2018) for residential constructions, where this type of intensity was useful because it helped to measure the hydrodynamic force of the flow over the buildings. The flow volume has also been considered, for example, in the curves developed by Winter et al. (2013, 2014) for low and high-speed roads, which model analysis and damage state were related directly to the debris flow volume deposited at the level of the road. Finally, the flow height has also been used for the development of fragility curves of debris flows, as is the case of Dagá et al. (2018), who developed fragility curves for bridges subjected to lahar flows. Flow height was included in the hydrodynamic force acting in the bridge deck sliding and substructure overturning models. Also Nieto et al. (2021) used the flow height in their fragility curves developed for road embankments exposed to perpendicular debris flows. Flow height plays a key role in their models because, when it exceeded embankment height, the headcut erosion phenomena was activated. The choice of the intensity measure depends on how it affects damage models and the practices of data collection. Measurement of flow height is relevant for flows running adjacent to road embankments because is involved in erosion process.

Formulation of the road embankment damage model

Definition of damage states. The damage is modeled for two types of roads: two-lane rural roads, with one lane in each direction, and multilane roads, having

two lanes per direction. Usually, the embankment foundation is composed of natural terrain, and it is exposed directly to the flows. Over this is constructed the road embankment, composed of specific soil. For this study, the road embankment is considered a body of homogeneous granular material, without distinguishing between upper layers of asphalt or concrete and different materials corresponding to natural terrain and fill of the embankment.

It was assumed in the modeling that the only difference between two-lane rural roads and multilane roads is the lane and lateral clearance width, because damage states were defined in terms of this measure. Other types of differences were not included. These measures are defined for each type of road below and guided by parameters used by Nieto et al. (2021). The platform width considers lane width (b_{lane}) and lateral clearance. The lateral clearance is the sum of the outer shoulder width, platform crown over-width, and platform base over-width; this last width is calculated from the slope angle α and the height of the embankment (See Figure 2). For multilane roads, the inner shoulder width and median width are added. The damage states are defined in terms of traffic capacity loss ex-post the occurrence of the event, depending on the physical damage of the embankment (See Table 1). For damaged roads, it is usually more useful to consider three damage states due to their relationships with the traffic capacity decrease. In this case, the extensive damage state is intrinsically considering the complete damage state, similar to that defined in Winter et al. (2014). The damage is quantified in terms of the portion r_B of the crown of the missing embankment, which depends on platform width and the number of lanes. The damage is applied in the complete embankment height; r_B values obtained in each iteration are compared with ranges of the damage states as explained in Figure 3.

Limit state function (LSF)

Damage is considered in terms of a Limit State Function (LSF), which defines a failure criterion in function of all variables involved in the damage model. It is useful to evaluate the performance of structures subjected to different stresses. Limit state function is included in the analytical method for the definition of fragility curves and considers the definition of a limit state function, an equation used to evaluate the limit performance of the infrastructure, and relates the mechanical properties that give capacity to the element with those properties that define the demand or stress function (Allsop et al., 2007; Pitilakis et al., 2014). The form of the limit state function is presented in equation (1) as $Z(\widehat{X})$ and corresponding to a difference between $S(\widehat{X})$, the function that expresses the debris flow demand stresses over the structure of the embankment, and $R(\widehat{X})$, the function that represents the resistant stresses of the embankment. When the demand stresses exceed the resistant stresses, the limit state function takes a value ≤ 0, which means that the system is failing. Another way to define the limit state function is in terms of a Safety Factor (S.F.) that relates the ratio between $R(\widehat{X})$ and $S(\widehat{X})$, considering the system is failing if $S.F. \leq 1$ as seen in equation (2). The vector $(\widehat{X})$ contains all the variables that determine $R(\widehat{X})$ and $S(\widehat{X})$, which can be deterministic or probabilistic nature.

$$Z(\widehat{X}) = R(\widehat{X}) - S(\widehat{X}) \leq 0 \tag{1}$$

$$S.F. = \frac{R(\widehat{X})}{S(\widehat{X})} \leq 1 \tag{2}$$

The failure probability P_F is obtained from the limit state function as shown in equations (3) and (4). The failure or exceedance probability of the system is associated with an intensity measure of the natural hazard. This probability considers the flow height as an appropriate intensity measure for this research because the erosive processes depend directly on this hydrodynamic variable, and it is simple to measure in the field.

$$P_F = P\left(R(\widehat{X}) \leq S(\widehat{X})\right) = P\left(R(\widehat{X}) - S(\widehat{X}) \leq 0\right) \tag{3}$$

$$P_F = P\left(R(\widehat{X}) \leq S(\widehat{X})\right) = P\left(\frac{R(\widehat{X})}{S(\widehat{X})} \leq 1\right) \tag{4}$$

Analytical formulation of the LSF using bank erosion and block instability model

The model developed below is considered applicable to clear water flows with sediment concentration close to 0%, and for debris flows with sediment concentration less than 80%, avoiding its application in massive movements or landslides. The adjacent flow exerts shear stress along the entire exposed bank of the embankment. As shown in Figure 2, the ADEF block of instability is generated from the $\overline{AC}$ section up to its projection on the surface of the embankment, in the $\overline{FE}$ section, which is defined as r_B. Adjacent bank erosion and block instability occurs when the demanding forces $S_S(\widehat{X})$ that generate the failure exceed resistant forces $S_R(\widehat{X})$ that oppose the sliding of the ADEF block. The limit state function $Z(\widehat{X})$ is defined in terms of a Safety Factor (SF) between $S_R(\widehat{X})$ and $S_S(\widehat{X})$. Therefore, the system is failing if $Z(\widehat{X})$ is less than or equal to 1 as seen in equation (5). In equation (6), the resistant forces $S_R(\widehat{X})$ are composed by the shear force of the soil that depends on the normal stress σ_{soil} , the $\tan(\phi)$, and the area in which it is applied. This last one is considering the embankment height h_{emb} and the unit portion of the analysis $L_{portion}$. The soil friction angle is denoted by ϕ. In the following analysis, the debris flow height was defined as h_{flow} and for simplicity, it will be mentioned as flow height. The demanding forces $S_S(\widehat{X})$, includes the soil weight in terms of the specific weight of the embankment soil γ_{emb}, and the volume of the block that could fail denoted by V_{CEFG}, as seen in equation (7).

$$Z\left(\widehat{X}\right) = S.F. = \frac{S_R\left(\widehat{X}\right)}{S_S\left(\widehat{X}\right)} \tag{5}$$

$$S_R\left(\widehat{X}\right) = \sigma_{soil} \cdot \tan(\phi) \cdot h_{emb} \cdot L_{portion} \tag{6}$$

$$V_{CEFG} = h_{emb} \cdot r_B \cdot L_{portion} \tag{7}$$

$$If\ \ h_{flow} \leq h_{emb} : S_s\left(\widehat{X}\right) = \gamma_{emb} \cdot V_{CEFG} \tag{8}$$

$$\begin{aligned} If\ \ h_{flow} > h_{emb} : S_S\left(\widehat{X}\right) &= \gamma_{emb} \cdot V_{CEFG} \\ &+ \gamma_{flow} \cdot \left(h_{flow} - h_{emb}\right) r_B \cdot L_{portion} \end{aligned} \tag{9}$$

The instability of the ADEF block is calculated by assuming that a constant inclination angle is maintained and the loss of material is equal to the basal erosion of the block, a strictly valid assumption for uniform, non-cohesive banks with planar failure (Lai, 2017). For cases where the flow height h_{flow} is less than or equal to the embankment height h_{emb}, it is considered a demanding force only at the CEFG block weight as seen in equation (8). When the flow height exceeds the embankment height h_{emb}, a component associated with the flow weight is added to the demanding forces in terms of the specific weight of the flow γ_{flow} as seen in equation (9). In this case, the flow height h_{flow} over r_B is assumed as the difference between the free surface elevation and embankment height. The damage model also considered a unit width $L_{portion}$ for the embankment portion defined in the analysis (length in the outgoing plane in Figure 2).

To check the limit state function $Z(\widehat{X})$, it is necessary to obtain the width r_B that is lost as a product of the erosion and fall of the CEFG block. Partheniades' (1965) expression was used to model erosion, which defined an erosion rate ε (m/s) in terms of excessive shear stress. In equation (10), $B_{\perp}$ (m) is the normal distance that erodes at the toe of the embankment in a time interval Δt (s)$\cdot$ k_d $(m^3N^{-1}S^{-1})$ is the erodibility coefficient, τ_o (Pa) is the average of flow shear stress and τ_c^w (Pa) is the critical shear stress of the eroded soil and is considered the erodibility coefficient in terms of critical shear stress according to $k_d = 2 \cdot 10^{-7} \cdot \tau_c^{-0.5}$ (Midgley et al., 2012). The flow is considered under hydraulically rough conditions such that the critical shear stress τ_c defined in equation (11) is expressed in terms of the Shields parameter, considered constant for the coarse material of the embankment, which is approximately equal to 0.047 (Julien, 1995; Sturm, 2001). D_{50} is the median diameter of the particle, which in this case for coarse granular soil is considered equal to 2 mm (Verruijt, 2018). Considering the effect of the

embankment inclination, incorporating the gravity effects on the critical shear stress, and multiplying by a factor that includes the angle of the embankment soil ϕ and the embankment slope α, obtains the critical shear stress on the wall τ_c^w showed in the equation (12) (Julien, 1995; Sturm, 2001).

$$B_{\perp} = \varepsilon \cdot \Delta t = k_d \cdot \left(\tau_o - \tau_c^w\right) \cdot \Delta t \tag{10}$$

$$\frac{\tau_c}{\left(\gamma_{emb} - \gamma_{flow}\right) \cdot D_{50}} \approx 0.047 \tag{11}$$

$$\tau_c^w = \tau_c \cdot \sqrt{\frac{\sin^2 \alpha}{\sin^2 \phi}} \tag{12}$$

The shear stress distribution assumes the definition of Lai (2017), considering that the shear stress decreases linearly from the base of the embankment slope at point C to the surface of the flow that is in contact with the embankment slope at point D. The maximum shear stress τ_o^w (Pa) exerted by the flow on the wall of the embankment is defined in equation (13).It is considered in terms of the specific weight of the flow $\gamma_{flow}(kN \cdot m^{-3})$, the bed slope s, and the flow height h_{flow}, valid expression for straight trapezoidal channels (Julien, 1995). For clear water flows, γ_{flow} will be equal to 9.8 $(kN \cdot m^{-3})$. However, the results presented considered γ_{flow} between 13 and 23 $(kN \cdot m^{-3})$ approximately, considering the sediment concentration described in the scope of the model.

$$\tau_o^w = 0.75 \cdot \gamma_{flow} \cdot h_{flow} \cdot s \tag{13}$$

In channels with curvature, there have been relations to represent the increase on the wall shear-stress to consider the effects of secondary currents. Here it is implemented in the relationship proposed by the Federal Highway Administration of USA (Kilgore and Cotton, 2005), defining the increase of the shear stress by a factor K_b, a function of a range of radius of curvature. Considering the case of greater curvature, K_b takes a value equal to 2, and then the shear stress in bend zones τ_o^b is defined in equation (14).

$$\tau_o^b = K_b \cdot \tau_o^w \tag{14}$$

The case of both the flow in a straight zone and in a bend zone of the channel are included in the analysis, using the equation (10) with shear stress τ_o^w and τ_o^b, respectively. The above allows calculating the $B_{\perp}$ used to obtain the r_B width defined by Lai (2017) in equation (15).

Table 1. Damage states considered for calibration of fragility curves for adjacent erosion model. Modified from Nieto et al. (2021).

Damage state i	Ranges for r_B	Two-lane rural road	Multilane road
Slight Damage			
Low to null probability of capacity reduction	$r_B \leq$ *lateral clearance width*	Erosion causes damage within the lateral clearance, without lane damage	Erosion causes damage within the lateral clearance, without lane damage
Moderate Damage			
Probability of capacity reduction up to 50%	lateral clearnce width $< r_B \leq b_{lane}$	Erosion causes damage in the closest lane to the flow, resulting in partial or complete closure of one traffic direction	Erosion causes damage in one or both closest lanes resulting in partial or complete closure of one traffic direction
Extensive Damage			
Probability of capacity reduction greater than 50%	$b_{\text{lane}} < r_B$	Erosion causes damage in both lanes resulting in partial or complete closure of both traffic directions	Erosion causes damage in more than two lanes resulting in partial or complete closure of both traffic direction

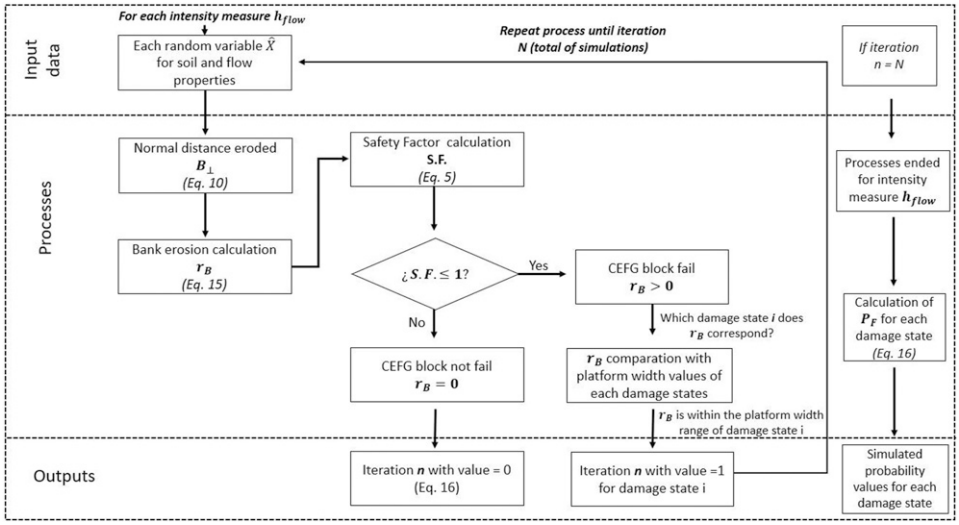

Figure 3. Flowchart of the analysis developed.

$$r_B = 0.5\frac{\left(h_{flow} + B_\perp \cdot \cos(\alpha)\right) \cdot \left(B_\perp \cdot \sin(\alpha) + \frac{B_\perp \cdot \cos(\alpha)}{\tan(\alpha)}\right)}{h_{emb} + B_\perp \cdot \cos(\alpha)} \tag{15}$$

After calculating r_B for each type of road, it is classified in one of the three damage states defined in Table 1. This process is performed randomly and repeated several times for each flow intensity measure, as explained in the following section and as summarized in Figure 3.

Development of fragility curves by simulation

Monte Carlo simulations for calibration of fragility curves. Monte Carlo simulations are considered in the analysis for the evaluation of the limit state function and the calculation of the embankment width r_B that is lost. This method generates different hazard and infrastructure response scenarios through the variability of the components defined in the conceptual model and limit state function. Each random variable $(\widehat{X})$ is sampled based on its deterministic value or probabilistic distribution assigned, on which the limit state function depends. When the function $Z_i(\widehat{X})$ is ≤ 1 in the simulation i, the embankment loses a part of its body equal to the width r_B. 100,000 simulations were performed, and the number of times n that infrastructure reached a damage state was counted over the total of N simulations (Melchers and Beck, 2018). The failure probability P_F considering this process is expressed in equation (16) in terms of the number of times the system has failed.

$$P_F \approx P\left(Z_i\left(\widehat{X}\right) \leq 1 \middle| H = h_{flow}\right) = \frac{n\left(Z_i\left(\widehat{X}\right) \leq 1\right)}{N} \tag{16}$$

Based on field data from events that occurred in Chile, it was considered a realistic scenario to have flow height h_{flow} from 0 to 8 m, increased in ranges equal to 0.25 m. To ensure convergence of probabilities P_F and corroborate that the number N of simulations as sufficient, the Coefficient of Variation (CV) was calculated for low flow heights (those involving low probabilities), resulting in a value less than 5%.

Table 2. Variables $(\widehat{X})$ considered in limit state function.

Variable	Name	Unit	Probability distribution	Reference value
s	Bed slope	$\frac{m}{m}$	Uniform (0.001,0.1)	Orellana et al. (2017); Sepúlveda et al. (2006); Sepúlveda et al. (2014)
α	Embankment slope angle	°	33.69	MOP (2020)
γ_{flow}	Debris flow specific weight	$\frac{kN}{m^3}$	Log-normal (17.75, 1.15)	Takahashi (2014); Thouret et al. (2020)
h_{emb}	Embankment height	*m*	Uniform (1,2.5), Uniform (2.5,4), Uniform (4,6)	Assumption according to analysis
b_{lane}	Two-lane rural road width	*m*	Uniform (2, 3.5)	MOP (2020)
	Multilane road width	*m*	3.5	MOP (2020)
$b_{shoulder-outer}$	Two-lane rural road outside shoulder width	*m*	Uniform (0,1)	MOP (2020)
	Multilane road outside shoulder width	*m*	Uniform (1,2.5)	MOP (2020)
$b_{shoulder-inner}$	Multilane road inner side shoulder width	*m*	Uniform (0.6,1)	MOP (2020)
$b_{over-width}$	Platform crown over-width	*m*	Uniform (0.5,1)	MOP (2020)
b_{median}	Median width	*m*	Uniform (0,2)	MOP (2020)
γ_{emb}	Embankment soil specific weight	$\frac{kN}{m^3}$	Uniform (20,25.97)	Terzaghi et al. (1996); Verruijt (2018)
φ	Embankment soil friction angle	*rad*	Log-normal (33.23, 1.18)	Terzaghi et al. (1996)

Definition of variables involved in bank erosion and block instability model for simulation

Table 2 presents the variables used in the expressions of the limit state function $Z(\widehat{X})$ and the expressions used for the calculated r_B. Deterministic values are indicated when only one value is recommended in the literature. Uniform distributions are defined in those cases in which there are only extreme values in the literature, or there were not enough data to be certain of the behavior of the variable. For debris flow specific weight, it was possible to adjust and check a log-normal distribution with the goodness of fit. As described in equation (10), a time interval Δt is required, which will, in this case be considered equal to 5 h, to evaluate the performance of the model. The embankment height considered in the study was divided into three ranges because the damage model developed presented sensitivity to this parameter.

Adjustment of a log-normal distribution to simulated curves

Sources recommend parameterizing known distribution to calculate the probability of exceeding a damage state for any flow height, and this procedure is often used in studies that develop fragility curves, regardless of the type of natural hazard (Shinozuka et al., 2000; Tsubaki et al., 2016). The cumulative log-normal distribution has been used in engineering as one of the functions that fit the obtained fragility curves, and their determination is simple because it depends only on two parameters $\widehat{\mu}$ and $\widehat{\sigma}$ (Nazari and Bargi, 2012; Porter, 2016). The Maximum Likelihood Estimation (MLE) is used for adjustment, which considers the calculation of an L function in terms of the specific fragility curves for each damage state as seen in equation (17), where if the term $x_i = 1$, means the damage state is reached, in otherwise, $x_i = 0$. Also, it is considered the n_i as the times the embankment is damaged over the total

times of the simulations N_i. After applying the method, it is important to find $\widehat{\mu}$ and $\widehat{\sigma}$ parameters that maximize the L function and are expressed in equation (18).

$$L = \Pi_{i=1}\left[F\left(h_{flow_i}\right)\right]^{x_i} \cdot \left[1 - F(h_{flow_i})\right]^{1-x_i} \quad (17)$$

$$\left\{\widehat{\mu},\widehat{\sigma}\right\} = argmax\left\{\sum_{i=1}\left[\left\{n_i \cdot \ln\left[\Phi\left(\frac{\ln\left(h_{flow_i}\right)-\widehat{\mu}}{\widehat{\sigma}}\right)\right]\right\} + (N_i - n_i)\cdot\ln\left\{1-\Phi\left(\frac{\ln(h_{flow_i})-\widehat{\mu}}{\widehat{\sigma}}\right)\right\}\right]\right\} \quad (18)$$

Chi-Square goodness of fit test was performed, checking with a 99.5% of confidence that the log-normal curves fit the simulation data. For each fragility curve, 32 simulated points were obtained. Considering two estimated parameters, the statistic associated with 29 degrees of freedom for a significance level of 0.5% is 52.34. A Chi-Square statistical test calculated from the difference between what was observed and what was expected, for all calculated distributions, was less than 0.3. This adjustment was made for the three embankment height ranges, which parameters are shown in Table 3.

Results

Fragility curves for road embankments exposed to adjacent erosion

The following fragility curves are obtained for two-lane rural roads and multilane roads considering bend and straight zones of the channel. These were developed considering debris flows as the hazard flow. The curves presented in Figure 4 and Figure 5 correspond to the first range of embankment height. However, simulations and adjustments of log-normal distributions were performed for three embankment height ranges. The parameters of these log-normal distributions for all simulated curves are shown in Table 3.

Table 3. Parameters of the log-normal distribution adjusted to the curves.

			Straight zone channel		Bend zone channel	
Road type	h_{emp} range [m]	Damage state	μ	σ	μ	σ
Two-lane rural	1–2.5	Slight	−0.511	0.860	−0.916	0.850
		Moderate	0.199	0.750	−0.357	0.830
		Extensive	0.688	0.680	0.104	0.810
	2.5–4	Slight	0.215	0.760	−0.431	0.880
		Moderate	0.793	0.670	0.223	0.800
		Extensive	1.061	0.660	0.542	0.750
	4–6	Slight	0.668	0.700	−0.020	0.870
		Moderate	1.194	0.620	0.615	0.780
		Extensive	1.387	0.640	0.788	0.770
Multilane	1–2.5	Slight	−0.400	0.790	−0.916	0.830
		Moderate	0.500	0.700	−0.051	0.790
		Extensive	1.297	0.600	0.718	0.750
	2.5–4	Slight	0.223	0.750	−0.357	0.880
		Moderate	0.944	0.660	0.351	0.820
		Extensive	1.548	0.640	0.986	0.720
	4–6	Slight	0.641	0.740	0.010	0.860
		Moderate	1.308	0.650	0.765	0.760
		Extensive	1.705	0.550	1.194	0.700

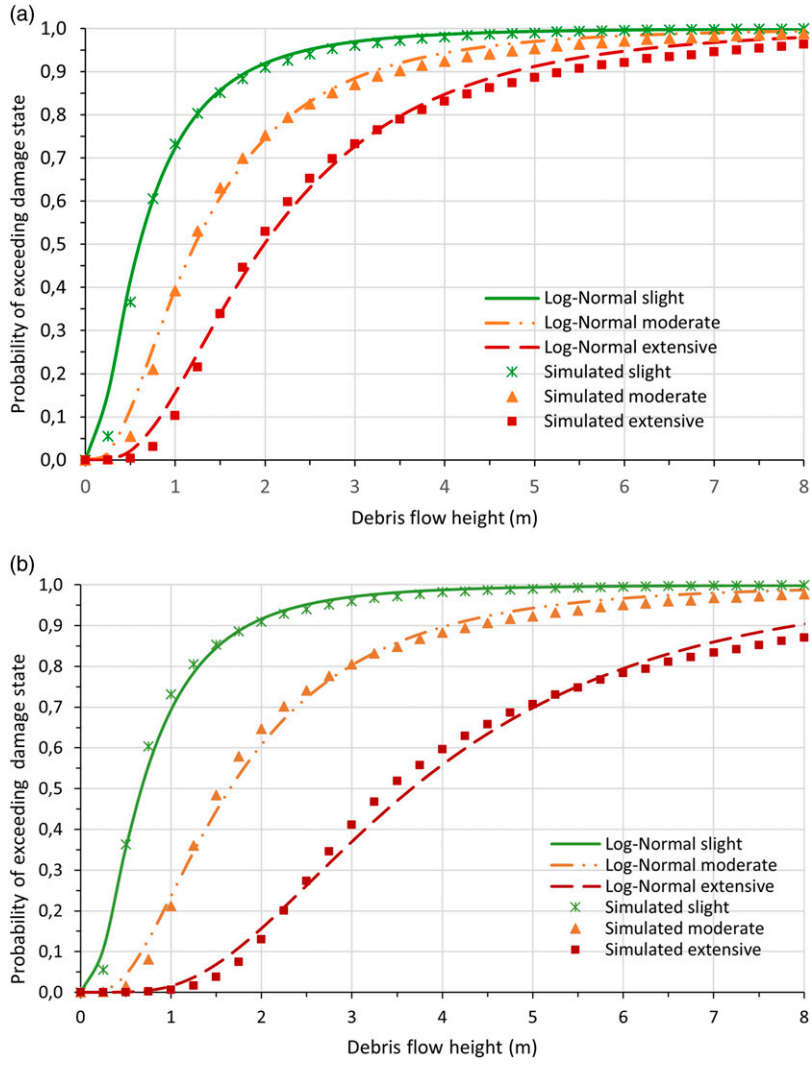

Figure 4. (a)Fragility curves for adjacent erosion in straight zones channel on two-lane rural roads with embankment height of 1–2.5 m, (b)Fragility curves for adjacent erosion in straight zones channel on multilane roads with embankment height of 1–2.5 m. For interpretation of the references to colours in this figure legend, refer to the online version of this article.

Discussion of analytical models and developed curves

Fragility curves are obtained from a model of bank erosion and block instability. The analysis was divided in two, considering straight and bend zones of the channel separately because the shear stress in bend channel sections is greater. The models also obtain different curves for two-lane rural roads and multilane roads because they have different platform widths. Therefore, the damage states and the consequent decrease in traffic capacity are also different. This procedure generates two curves for each type of road, which enables rigorous analysis of the damage considering the different erosive processes in bend and straight zones of channels and the three ranges of embankment height.

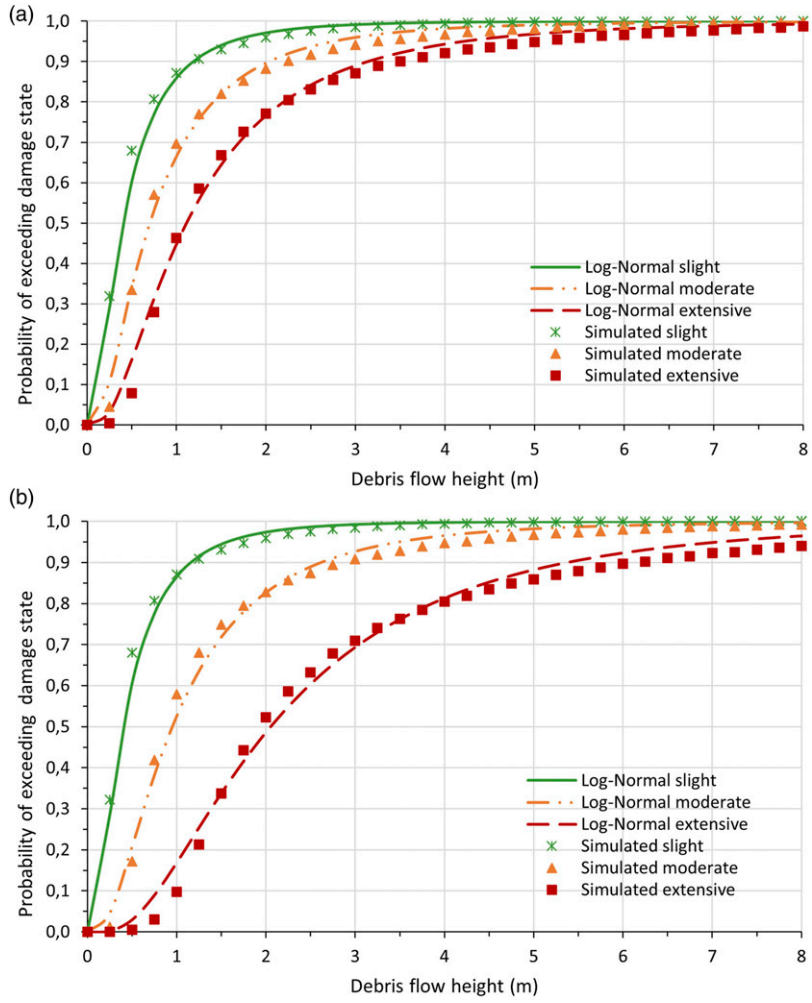

Figure 5. (a)Fragility curves for adjacent erosion in bend zones channel on two-lane rural roads with embankment height of 1–2.5 m, (b)Fragility curves for adjacent erosion in bend zones channel on multilane roads with embankment height of 1–2.5 m. For interpretation of the references to colours in this figure legend, refer to the online version of this article.

The expressions used in the models presented do not show limitations to be used in clear water flows or flows with low sediment concentration. Considering this last case would require a modification of the specific weight of the flow, an increase of the total volume as a function of concentration, and changes on the Manning coefficient (Contreras and Escauriaza, 2020), which could reduce the shear stress of the flow. However, it is always advisable to check the specific conditions and assumptions before applying these models. The limit state function defined in the study as a safety factor is used to check the block instability of r_B width, but for the fragility curves construction, the comparison between r_B width was used with road platform width.

The 5-h interval considered in the analysis evaluates the performance of the damage model. However, it is possible to adjust this modeling approach to any required time interval. For longer interaction times, bank erosion will be greater, and

the probability of damage will increase, so the curves would be expected to move to the left. When this happens, the curves become more deterministic than probabilistic because the log-normal curve slope increases and thus resembles a step function. The result would obtain the total failure of the road embankment rather than various intermediate damage states.

Only log-normal curves are shown for the lower embankment height ranges. It is important to mention that for larger embankment heights, i.e. for the second and third range of the embankment height (2.5–4 m and 4–6 m), the probability of exceeding some damage states decreases. The above is consistent with equation (15) used to calculate the lost platform width r_B because the expression is inversely proportional to the embankment height. On the other hand, if the functions established for straight zones of the channel are compared with those valid for bend zones, considering the same type of road, note that the effects of channel curvature and secondary currents produce a higher probability of exceeding a damage state. For example, the debris flow height is set at 2 m, the graph in Figure 4(a) shows a probability of exceeding a moderate damage state approximately equal to 75%. In contrast, the graph in Figure 5(a) for the same flow height and damage state has 90% probability of exceedance.

Comparing the probability for the same intensity measure in two-lane rural roads and multilane roads, note that the first type of road has a higher chance of damage than the second type. The defined damage states explain this because these compare the lost width r_B due to adjacent interaction flow with the total width of the road platform. Thus, larger platform widths (associated with multilane roads) will be less affected in capacity to transport vehicles than smaller platform widths (associated with two-lane rural roads). The analysis showed that two-lane rural roads are more likely to reduce their capacity by at least 50% than multilane roads.

Conclusions

This research provides a methodology for developing fragility curves for road embankments exposed to adjacent flows by defining a damage model that includes the erosion of the embankment slope and the instability of the weight of the same embankment. The following findings and conclusions were derived from this study:

Despite the advances in the development of probabilistic models for road networks exposed to debris flows, studies were inconclusive regarding road embankments. Nieto et al. (2021) advanced probabilistic models for the perpendicular exposure of these embankments, but the physical damage generated by flow adjacent to roads had not been analyzed previous to this study. The damage models identified and developed in this research allow stakeholders and decision-making to take preliminary measures both in the design and management of road networks exposed to flows. In turn, fragility curves are a key tool in quantifying the physical risk of roads exposed to natural hazards; so, their ultimate purpose is to provide information for decision-making regarding restoration and mitigation measures, advancing resilient road networks.

Through the definition of limit state function, three damage states, and considering erosion and instability models, the fragility curves presented were obtained from 100,000 Monte Carlo simulations. They enabled calculation of the platform width r_B that was lost for each one. Subsequently, log-normal distributions were adjusted for simulation data, fulfilling the research aim.

The geometric characteristics of each embankment have a direct influence on its fragility. Higher embankments are less fragile to the exposure of adjacent flows than lower embankments. In turn, two-lane rural embankments associated with smaller platform widths are more fragile than multilane embankments associated with larger platform widths. The decrease in the capacity of transport of roads depends directly on the damage affecting road embankments exposed to adjacent flows and their fragility. Two-lane rural roads have a higher probability of reducing their capacity by at least 50% than multilane roads for the same intensity measure of flow.

The study recognized that embankments exposed to a debris flow in bend zones of channels realize greater damage than those adjacent to straight zones.

The erosive capacity of the flow defined in terms of the flow shear stress is directly increased by secondary currents that are generated at the outer bend of the flow resulting from cross-stream pressure gradients.

This study validated with 99.5% confidence that log-normal distributions adjusted to the functions obtained from the Monte Carlo simulations were highly useful in calculating the probability of exceedance for any flow height. However, it should be recognised that the curves presented here were generated from simulations with 5 h of interaction time; so, when it is required to know the specific behavior for other time periods, it is necessary to run new simulations.

The presented damage model is applicable to water flows and debris flows, considering a sediment concentration less than 80% for the debris flows. Fragility curves are an input tool for quantitative risk assessment of road networks exposed to these flows. To use these models, reviewing the geometric and design considerations and making the necessary adjustments for their application in different areas than considered in this study are recommended. Each case is specific to the conditions of the road, embankment, and flow.

For this research, very few empirical data were available to validate the curves developed. Thus, it is important to advance in damage data collection mechanisms for natural hazards. An important future research line includes validating the curves presented in this study with empirical data and measuring them against situations with clear water flows. It would be convenient to advance in other mechanisms of analysis for comparing the results obtained, for example, with finite element modeling that enables verifying analytically the models of damage proposed. Also, it would be useful to use finite element modeling to capture the heterogeneity of the soil embankment and to evaluate whether it affects the model proposed. In addition, future research should analyze all the damage models developed for road embankment exposure to debris flows, including the effect of coupling perpendicular and adjacent models.

Flow height has been considered as the intensity measure of the flow in the models presented. Regardless of the phenomenon that triggers the flows, the curves will be useful to calculate the probability of damage. However, it is convenient to evaluate, in future research, possible incidences of climate change in the models, considering that increasingly extreme natural events should be expected, which may require larger intensity measurement for fragility curves. These road networks are important social and economic facilitators and learning how to protect them from damage is important to every government and citizen; understanding damage to embankments from flow is one element of road construction and maintenance that deserves more attention and study.

Declaration of conflicting interests

The author(s) declared no potential conflicts of interest with respect to the research, authorship, and/or publication of this article.

Funding

The author(s) disclosed receipt of the following financial support for the research, authorship, and/or publication of this article: This work was supported by the Research Center for Integrated Disaster Risk Management (CIGIDEN) (grant no. ANID/FONDAP/15110017), FONDECYT Project (grant no. 1181754/FONDECYT/ANID), FONDEF Project Research and Development of Models to Quantify and Mitigate the Risk of Natural Hazards in the National Road Network (grant no. ID14I20309/Fondef/ANID).

ORCID iD

Alondra Chamorro https://orcid.org/0000-0001-9466-6468

References

Allsop W, Kortenhaus A and Morris M (2007) Failure mechanisms for flood defence structures. Report for the FLOODsite project. Report T04-06-01. Available at: http://hikm.ihe.nl/floodsite/data/Task4/pdf/failmechs.pdf.

Argyroudis S and Kaynia AM (2014) Fragility functions of highway and railway infrastructure. In: Pitilakis K, Crowley H and Kaynia AM (eds), *SYNER-G:*

Typology Definition and Fragility Functions for Physical Elements at Seismic Risk: Buildings, Lifelines, Transportation Networks and Critical Facilities. Netherlands: Springer, pp. 299–326.

Argyroudis S and Kaynia AM (2015) Analytical seismic fragility functions for highway and railway embankments and cuts. *Earthquake Engineering & Structural Dynamics* 44: 1–6. DOI: 10.1002/eqe.

Argyroudis S, Mitoulis S, Kaynia AM, et al. (2018) Geotechnical Earthquake Engineering and Soil Dynamics. In: *Fragility Assesment of Transportation Infrastructure Systems Subjected to Earthquakes*.

Argyroudis S, Mitoulis S, Winter MG, et al. (2019) Fragility of transport assets exposed to multiple hazards: State-of-the-art review toward infrastructural resilience. *Reliability Engineering and System Safety*, 191. DOI: 10.1016/j.ress.2019.106567.

Calvo B and Savi F (2009) A real-world application of Monte Carlo procedure for debris flow risk assessment. *Computers and Geosciences* 35(5): 967–977. DOI: 10.1016/j.cageo.2008.04.002.

Contreras MT and Escauriaza C (2020) Modeling the effects of sediment concentration on the propagation of flash floods in an Andean watershed. *Natural Hazards and Earth System Sciences* 20(1): 221–241.

Crosato A (2007) Effects of smoothing and regridding in numerical meander migration models. *Water Resources Research* 43(1): 1–10. DOI: 10.1029/2006WR005087.

Dagá J, Chamorro A, De Solminihac H, et al. (2018) Development of fragility curves for road bridges exposed to volcanic lahars. *Natural Hazards and Earth System Sciences* 18(8): 2111–2125. DOI: 10.5194/nhess-18-2111-2018.

Dilley M, Chen RS, Deichmann U, et al. (2005) Natural disaster hotspots: A global risk analysis. *Report for World Bank. Disaster Risk Management Series*. Washington DC, 5.34423.

Dowling CA and Santi PM (2014) Debris flows and their toll on human life: A global analysis of debris-flow fatalities from 1950 to 2011. *Natural Hazards* 71(1): 203–227. DOI: 10.1007/s11069-013-0907-4.

Gouldby B, Sayers P and Hassan M (2009) *A Methodology for Regional-Scale Flood Risk Assessment*. Proceedings of the Institution of Civil Engineers. Water Management 000: 1–14 DOI: 10.1680/wama.2009.00084.

Hungr O, Leroueil S and Picarelli L (2014) The Varnes classification of landslide types, an update. *Landslides* 11(2): 167–194. DOI: 10.1007/s10346-013-0436-y.

Jakob M and Hungr O (2005) *Debris-flow Hazards and Related Phenomena*. Chichester: Springer and Praxis. DOI: 10.1017/CBO9781107415324.004.

Julien P (1995) *Erosion and Sedimentation*. Cambridge: Cambridge University Press. DOI: 10.1017/CBO9781139174107.

Kilgore R and Cotton G (2005) Design of Roadside Channels with Flexible Linings. In: *Repor for Federal Highway Administration. Report No. FHWA-NHI-05-114, April*. Washington DC, USA.

Kim H, Sim SH, Lee J, et al. (2017) Flood fragility analysis for bridges with multiple failure modes. *Advances in Mechanical Engineering* 9(3): 1–11. DOI: 10.1177/1687814017696415.

Lai YG (2017) Modeling stream bank erosion: Practical stream results and future needs. *Water* 9(12): 950. DOI: 10.3390/w9120950.

Liang Y and Xiong F (2019) Quantification of debris flow vulnerability of typical bridge substructure based on impact force simulation. *Geomatics, Natural Hazards and Risk* 10(1): 1839–1862. DOI: 10.1080/19475705.2019.1641564.

Mavrouli O, Fotopoulou S, Pitilakis K, et al. (2014) Vulnerability assessment for reinforced concrete buildings exposed to landslides. *Bulletin of Engineering Geology and the Environment* 73: 265–289.

McKenna G, Argyroudis S, Winter MG, et al. (2021) Multiple hazard fragility analysis for granular highway embankments: Moisture ingress and scour. *Transportation Geotechnics* 26(September 2020): 100431. DOI: 10.1016/j.trgeo.2020.100431.

Melchers R and Beck A (2018) Integration and Simulation Methods. In: Melchers R and Beck A (eds), *Structural Reliability: Analysis and Prediction*. NJ: John Wiley & Sons. 63–93 DOI: 10.1002/9781119266105.

Meyer NK, Schwanghart W, Korup O, et al. (2015) Roads at risk: Traffic detours from debris flows in southern Norway. *Natural Hazards and Earth System Sciences* 15(5): 985–995. DOI: 10.5194/nhess-15-985-2015.

Midgley TL, Fox GA and Heeren DM (2012) Evaluation of the bank stability and toe erosion model (BSTEM) for predicting lateral retreat on composite streambanks. *Geomorphology* 145(146): 107–114. DOI: 10.1016/j.geomorph.2011.12.044.

MOP (2020) *Manual de Carreteras Volumen 3 - Instrucciones y Criterios de Diseño*. Chile: ReportMinistry of Public Works.

Motta D, Abad JD, Langendoen EJ, et al. (2012) A simplified 2D model for meander migration with physically-based bank evolution. *Geomorphology* 163: 164–225. DOI: 10.1016/j.geomorph.2011.06.036.

Nazari YR and Bargi K (2012) Practical approach to fragility analysis of bridges. *Research Journal of Applied Sciences, Engineering and Technology* 4(23): 5177–5182.

Nettleton IM, Martin S, Hencher S, et al. (2005) Debris flow types and mechanisms. In: *Report, Scottish Road Network Landslides Study, Scotland*. Available at: http://www.scotland.gov.uk/Publications/2005/07/08131738/17395

Nieto N, Chamorro A, Echaveguren T, et al. (2021) Development of fragility curves for road embankments exposed to perpendicular debris flows. *Geomatics, Natural Hazards and Risk* 12(1): 1560–1583. DOI: 10.1080/19475705.2021.1935330.

Oblak A, Kosic M, Viana Da Fonseca A, et al. (2020) Fragility Assesment of Traffic Embankment Exposed to Earthquake-Induced Liquefaction. *Applied Sciences* 10(19): 6832.

Orellana H, García JL, Ramírez C, et al. (2017) El aluvión del 9 agosto 2015 en Alto Patache, región de Tarapacá, Desierto de Atacama. *Revista de Geografia Norte Grande* 89(68): 65–89. DOI: 10.4067/S0718-34022017000300065.

Partheniades E (1965) Erosion and deposition of cohesive soils. *Journal of the Hydraulics Division* 91(1): 105–139.

Peduto D, Ferlisi S, Nicodemo G, et al. (2017) Empirical fragility and vulnerability curves for buildings exposed to slow-moving landslides at medium and large scales. *Landslides* 14(6): 1993–2007. DOI: 10.1007/s10346-017-0826-7.

Pitilakis K, Crowley H and Kaynia AM (2014) Introduction. In: Pitilakis K, Crowley H and Kaynia AM (eds), *SYNER-G: Typology Definition and Fragility Functions for Physical Elements at Seismic Risk: Buildings, Lifelines, Transportation Networks and Critical Facilities*. NetherlandsUSA: SpringerReport, University of Colorado Boulder, pp. 1–28. Porter K (2016 DOI: 10.1007/978-0-387-93837-0.

Porter K. (2016) *A Beginner ' S Guide to Fragility , Vulnerability , and Risk*. DOI: 10.1007/978-0-387-93837-0.

Prieto JA, Journeay M, Acevedo AB, et al. (2018) Development of structural debris flow fragility curves (debris flow buildings resistance) using momentum flux rate as a hazard parameter. *Engineering Geology* 239: 144–157. DOI: 10.1016/j.enggeo.2018.03.014.

Santi PM, Hewitt K, VanDine DF, et al. (2010) Debris-flow impact, vulnerability, and response. *Natural Hazards* 56(1): 371–402. DOI: 10.1007/s11069-010-9576-8.

Schultz MT, Gouldby BP, Simm JD, et al. (2010) *Beyond the Factor of Safety : Developing Fragility Curves to Characterize System Reliability*. USA, July: Report, US Army Corps of Engineers.

Scott DM, Novak DC, Aultman-Hall L, et al. (2006) Network Robustness Index: A new method for identifying critical links and evaluating the performance of transportation networks. *Journal of Transport Geography* 14(3): 215–227. DOI: 10.1016/j.jtrangeo.2005.10.003.

Sepúlveda S, Rebolledo S, McPhee J, et al. (2014) Catastrophic, rainfall-induced debris flows in Andean villages of Tarapacá, Atacama Desert, northern Chile. *Landslides* 11(3): 481–491. DOI: 10.1007/s10346-014-0480-2.

Sepúlveda S, Rebollledo S and Vargas G (2006) Recent catastrophic debris flows in Chile: Geological hazard, climatic relationships and human response. *Quaternary International* 158(1): 83–95. DOI: 10.1016/j.quaint.2006.05.031.

Shinoda M, Nakajima S, Watanabe K, et al (2021) Practical seismic fragility estimation of unreinforced and reinforced embankments in Japan. *Geosynthetics International* 28(1): 48–64. DOI: 10.1680/jgein.20.00026.

Shinozuka M, Feng M, Lee J, et al. (2000) Statistical analysis of fragility curves. *Journal of Engineering Mechanics* 126126: 1224–1231.

Simon A (2010) *2nd Joint Federal Interagency Conference*. In: Iterative bank-stability and toe-erosion modeling for predicting streambank loading rates and potential load reductions.

Simon A, Curini A, Darby SE, et al. (2000) Bank and near-bank processes in an incised channel. *Geomorphology* 35(3–4): 193–217. DOI: 10.1016/S0169-555X(00)00036-2.

Simon A (2011) Pollen-Bankhead N and Thomas RE-Development and application of a deterministic bank

stability and toe erosion model for stream restoration. *Geophysical Monograph Series* 194: 453–474. DOI: 10.1029/2010GM001006.

Skilodimou H and Bathrellos G (2016) *Debris Flow: Categories, Characteristics, Hazard Assessment, Mitigation Measures*. Report, Erasmus Programme of the European Union. Available at: https://eclass.uoa.gr/modules/document/file.php/GEOL312/Landslides/McAgenda_Text_debris_flow_final.pdf

Sturm T (2001) *Open Channel Hydraulics*. Boston: McGraw-Hill.

Tacnet JM, Mermet E and Maneerat S (2012) Analysis of importance of road networks exposed to natural hazards. In: Proceedings of the AGILE 2012 International Conference on Geographic Information Science February: 24–27.

Takahashi T (2014) *Debris Flow: Mechanics, Prediction and Countermeasures*. London: CRC Press.

Terzaghi K, Peck R and Mesri G (1996) *Soils Mechanics in Engineering Practice*. New York: John Wiley & Sons.

Thouret JC, Antoine S, Magill C, et al. (2020) Lahars and debris flows: Characteristics and impacts. Earth-Science Reviews, 103003. DOI: 10.1016/j.earscirev.2019.103003.

TRB (2016) *Highway Capacity Manual. A Guide for Multimodal Mobility Analysis*. Washington D.C.,USA: Report, Transportation Research Board.

Tsubaki R, Bricker JD, Ichii K, et al. (2016) Development of fragility curves for railway embankment and ballast scour due to overtopping flood flow. *Natural Hazards and Earth System Sciences* 16(12): 2455–2472. DOI: 10.5194/nhess-16-2455-2016.

Verruijt A (2018) *An Introduction to Soil Mechanics*. Delft: Springer. DOI: 10.1007/978-3-319-61185-3.

Watson AJ and Basher LR (2006) Stream bank erosion: a review of processes of bank failure, measurement and assessment techniques, and modeling approaches. Report, Landcare Research. New Zealand.

Winter M, Smith J, Fotopoulou S, et al. (2013) The physical vulnerability of roads to debris flow. *18th International Conference on Soil Mechanics and Geotechnical Engineering Paris* 2013: 2281–2284.

Winter M, Smith J, Fotopoulou S, et al. (2014) An expert judgement approach to determining the physical vulnerability of roads to debris flow. *Bulletin of Engineering Geology and the Environment* 73(2): 291–305. DOI: 10.1007/s10064-014-0570-3.

Winter MG, Peeling D, Palmer D, et al. (2019) Economic impacts of landslides and floods on a road network. *Acta Universitatis Carolinae, Geographica* 54(2): 207–220. DOI: 10.14712/23361980.2019.18.

Zou Q, Cui P, Zhou G, et al. (2018) A new approach to assessing vulnerability of mountain highways subject to debris flows in China. *Progress in Physical Geography* 42(3): 305–329. DOI: 10.1177/0309133318770985.